Wave energy resource assessment with AltiKa satellite altimetry: A case study at a wave energy site

Goddijn-Murphy, Lonneke; Martín Míguez, Belen; McIlvenny, Jason; Gleizon, Philippe

Published in:
Geophysical Research Letters

Publication date:
2015

AGU PUBLICATIONS

Geophysical Research Letters

RESEARCH LETTER
10.1002/2015GL064490

Key Points:
- SARAL\AltiKa can give estimates of wave period and wave power
- Our method can be used for coastal wave energy resource assessment
- One year of SARAL\AltiKa data gave a reasonable estimate

Correspondence to:
L. Goddijn-Murphy,
Lonneke.Goddijn-Murphy@uhi.ac.uk

Citation:
Goddijn-Murphy, L., B. Martín Míguez, J. McIlvenny, and P. Gleizon (2015), Wave energy resource assessment with AltiKa satellite altimetry: A case study at a wave energy site, *Geophys. Res. Lett.*, *42*, 5452–5459, doi:10.1002/2015GL064490.

Received 8 MAY 2015
Accepted 22 JUN 2015
Accepted article online 26 JUN 2015
Published online 14 JUL 2015

Wave energy resource assessment with AltiKa satellite altimetry: A case study at a wave energy site

Lonneke Goddijn-Murphy[1], Belén Martín Míguez[2,3], Jason McIlvenny[1], and Philippe Gleizon[1]

[1]Environmental Research Institute, UHI-NHC, Thurso, UK, [2]Centro Tecnológico Del Mar, Fundación, Vigo, Spain, [3]Now at EMODnet Secretariat, InnovOcean, Oostende, Belgium

Abstract A simple model to estimate wave power at a coastal site from satellite radar altimetry is proposed. We used data from the AltiKa altimeter on board the SARAL satellite because of its superior performance near the coast. The deep water approximation was applied to our 60 m deep site along with a simple empirical model to estimate wave period, T, from altimeter significant wave height, H_s, and backscattering coefficient, σ_0. A known relation between zero-crossing period, T_z, and wave energy period, T_E, was used in combination with H_s to calculate wave power per meter wave crest (P). The annual and seasonal mean values of P using AltiKa parameters largely agreed with known ranges of P at the site. A comparison with shallower sites and sites closer to the coast revealed that for estimation of T_z from AltiKa the water depth could be taken into account and an empirical relation is given.

1. Introduction

Recent advancements in satellite altimetry enable novel applications in coastal waters; this study presents an example of how they can be used in wave energy assessment near the coast. Applications of satellite altimetry over the open ocean are well established, but the measurements near the coasts have been largely rejected and flagged as "bad data." This is because of difficulties in the corrections and issues of land contamination in the footprint [*Cipollini et al.*, 2010]. Currently, these rejected data are being reprocessed using algorithms improved for the coastal zone and thereby filling the gaps that existed previously. An overview of these efforts is given by *Cipollini et al.* [2010]. In addition to the technological advancements of the data processing, satellite altimeters are being developed that perform better near the coast. One such satellite altimeter, the AltiKa altimeter on board the SARAL satellite, is subject of this paper. The SARAL mission was launched on 25 February 2013 with AltiKa the first Ka band (35 GHz) satellite altimeter. The higher frequency and several other AltiKa's attributes (larger bandwidth, smaller antenna beam width, higher pulse repetition frequency, and echo tracking) promise improved performance in coastal waters [*Raney and Phalippou*, 2011; *Sepulveda et al.*, 2015]. A recent assessment has confirmed that significant wave height, H_s, from AltiKa is more accurate near the coast than previous altimeters, particularly at low H_s [*Sepulveda et al.*, 2015]. We focus on the use of AltiKa for wave power estimation near the coast. Wave power is commonly expressed in terms of wave height and wave period, either through an equation or with the help of a look-up table (power matrix). Unlike wave height, wave period is not routinely measured with satellite altimeters, so we calculated wave period using a simple empirical model developed by *Gommenginger et al.* [2003] for the open ocean. For a comparison with in situ and known wave data we selected the location of a planned commercial scale (50 MW) wave energy farm in Farr Bay in the north of Scotland 10 km off the coast. At this site two waverider buoys are deployed (4.372°W, 58.632°N) and (4.239°W, 58.632°N) to assess the wave energy resource. In the area as well as high waves, strong tidal currents (peak flows of over 1 m/s [*ABPmer*, 2008]) can be expected. Because the calculation, particularly for the wave period, was expected to be specific to Farr Bay, a comparison was made with eight sites located in the North Sea off the coast of Netherlands.

2. Data Sources

2.1. AltiKa

The radar altimeter emits a pulse toward the Earth's surface and measures the backscatter. Nadir-looking altimeters were first developed to retrieve sea surface height, but the shape and size of the return signal,

the waveform, contain a lot more information about the ocean surface such as H_s, wave slope, and backscattering coefficient, σ_0. *Golubkin et al*. [2014] recently found proof that Ka band is more sensitive to changes in H_s than the traditionally used Ku band (13.6 GHz) using a direct comparison of wave measurements in wind seas. *Sepulveda et al*. [2015] confirmed that the standard deviation of the 1 Hz measurement of AltiKa H_s is much less than for other altimeters, particularly at low H_s (<0.5 m). They also show that SARAL/AltiKa performs better in a buoy comparison closer than 50 km to the coast than other altimeters (e.g., root-mean-square error, RMSE, of 22 cm and 26 cm for SARAL and Jason-2, respectively). *Gommenginger et al*. [2003] estimate wave period based on altimeters H_s and σ_0 using ~2.2 cm radar wavelength of the Ku band altimeter on board Topex, while AltiKa operates at the higher-frequency Ka band corresponding to shorter radar wavelength of ~0.8 cm. As microwaves are scattered by wave facets larger than about 3 times the incident wavelength, the AltiKa backscatter coefficient contains much more information relative to high-frequency components of the sea surface than Ku band. This could result in reduced sensitivity to the periods of larger sea surface waves. The main disadvantage of the Ka band is larger signal attenuation by atmospheric vapor and liquid water so that wave height estimates are sensitive to the presence of clouds and rain [*Tournadre et al*., 2009].

SARAL is a French (Centre National d'Etudes Spatiales, CNES)/Indian (Indian Space Research Organisation) collaborative mission to measure sea surface height using the Ka band and is expected to be operational for 3 years. We used the 1 s averages (1 Hz) of the Geophysical Data Records (GDRs) made freely available by CNES and AVISO (Archiving, Validation, and Interpretation of Satellite Oceanographic data) [*Bronner et al*., 2013] (40 Hz data are also available). The 1 s averages have a spatial resolution of 11 km (along) × 5 km (across). The SARAL passes are separated by about 40 km distance in Farr Bay, the distance between two 1 s samples is 7 km, and the repeat time of each pass is 35 days. The significant wave height data of the GDRs are corrected for instrument errors and system bias. We downloaded H_s and σ_0 data for AltiKa passes 143, 687, and 876 because these were the closest to the waverider buoys (excluding passes farther than 20 km), from cycles 9 to 19. For each pass we compared the AltiKa sample closest to the buoy location using the buoy measurement closest to the AltiKa sample time, and hence, we did not average over all samples within a 50 km radius around the buoy as is usually done for altimeter calibrations in the open ocean [e.g., *Queffeulou*, 2004; *Zieger et al*., 2009]. In the open ocean significant variability resulting from geophysical processes can be ignored, but at a coastal site significant variability is very likely. We therefore applied a point-by-point calibration (it should be noted that the sample points in themselves are averages). It implies that our calibration was possibly site specific.

2.2. Wave Data

Two-directional waverider buoys DWR-MkIII from Datawell were deployed in Farr Bay from 14 January to 16 July 2014 and from 2 October 2014 onward; wave data for this paper were downloaded on 5 January 2015. The wave buoys were moored 10 km off the coast, spaced 7.7 km apart, and the water depth was 60 m. In this paper we analyzed the half-hour averages provided by the waverider of H_s, zero-crossing period, T_z, mean period, T_m, and peak period, T_p, defined by equations (1)–(4),

$$H_s = 4\sqrt{m0} \tag{1}$$

$$T_z = \sqrt{m0/m2} \tag{2}$$

$$T_m = m0/m1 \tag{3}$$

$$T_p = 1/f_p \tag{4}$$

with the m's the moments of the power spectral density $S(f)$, and f_p the frequency at which $S(f)$ is maximal [*Holthuisen*, 2007]. The wave buoy's half-hour averages were calculated every 3 min (moving average), and we used the middle of the averaging period as the time stamp.

For a comparison with other sites we used wave measurement data from eight sites in the North Sea off the Dutch coast for the year 2014 obtained by request from the Ministry of Infrastructure and Environment (Rijkswaterstaat) in the Netherlands. The sites were 2 km to 160 km away from the shore, and the depths ranged from 6 m to 44 m (Table 1). We collocated their T_z and H_s measurements with those from AltiKa passes closer than 20 km and selected the in situ data closest to the overpass time. Five stations provided data every 10 min and three stations hourly.

Table 1. Linear Regression Results Between X (Equation (5)) Using Altimeter Data and In Situ T for (Top) *Gommenginger et al.* [2003], (Middle) Farr Bay and the Three Definitions of T, and (Bottom) Comparison Sites Off the Dutch Coast and T_z, With "d" Depth (m), "o" Distance to the Coast (km), N Number of Matches, and Δa and Δb the 95% Confidence Bounds of a and b

Station	T (s)	d	o	N	a	$\pm\Delta a$	b	$\pm\Delta b$	R^2
Open Ocean (G03)	$T_{z,b} = a\,X + b$	~4000		5075	2.545	0.045	−0.895	0.126	
Farr Bay		60	10	48					
	$T_{z,b} = a\,X + b$				1.86	0.40	1.15	1.05	0.65
	$T_{m,b} = a\,X + b$				2.16	0.56	1.25	1.47	0.56
	$T_{p,b} = a\,X + b$				2.76	1.36	3.16	3.54	0.27

						$T_{z,b} = a\,X + b$ (s)				
Station	Longitude	Latitude	d	o	N	a	$\pm\Delta a$	b	$\pm\Delta$b	R^2
F3PFM	4.73	54.86	44	160	20	1.79	0.34	0.86	0.88	0.87
IJMDMNTSPS	4.06	52.55	22.5	35	18	1.24	0.40	1.76	0.83	0.73
IJMDSMPL	4.52	52.46	14	2.5	20	0.95	0.78	2.40	1.45	0.27
EIELSGT	4.66	53.28	27	14	17	1.20	0.71	2.11	1.43	0.46
SCHIERMNOND	6.17	53.60	19	8	18	1.51	0.80	1.39	1.68	0.50
SCHIERMNOWG	6.16	53.53	6	2.5	20	0.74	1.00	2.97	2.19	0.12
WESTEOT	6.52	53.62	9	2	11	NaN	NaN	NaN	NaN	0.03
WESTEWT	6.37	53.62	13	10	22	1.22	0.62	1.95	1.33	0.46

3. Additional Wave Parameters From Altimetry

3.1. Wave Period

3.1.1. Existing Algorithms

Gommenginger et al. [2003] propose a simple empirical model, hereafter referred to as G03, to retrieve T from Ku band σ_0 and H_s. It is based on the approximations of (1) the inverse of σ_0 as the mean square slope (MSS) of the long ocean waves [*Barrick*, 1974], (2) the proportionality of the wave slope to the ratio of wave height and wavelength (L), and (3) $L \propto T^2$ for deep waters (section 3.1.2). Combining these three approximations gives $\mathrm{MSS} \propto H_S^2/T^4$ and $T \propto \left(\sigma_0 H_s^2\right)^{0.25}$. *Gommenginger et al.* [2003] therefore define a variable X

$$X = \left(\sigma_0 H_s^2\right)^{0.25} \tag{5}$$

and compare X derived from Topex altimeters σ_0 and H_s, with T_z, T_m, and T_p values from measurements of one-directional wave buoy spectra. The buoys were selected for their location in open water and proximity to Topex tracks, providing 6344 data points. Regarding approximation (1), it should be pointed out that MSS is proportional to the acceleration variance, which is the fourth moment of the wave spectrum [*Rascle and Ardhuin*, 2013], so σ_0 will be very sensitive to high-frequency wave components (short gravity waves) while the wave buoys measure waves in the order of meters as they are not capable of high-frequency measurements. This relationship between the contributions of longer swell waves and the short capillary gravity waves to the σ_0 signal is poorly understood, making an empirical approach necessary. *Quilfen et al.* [2004] have proposed a dual-frequency algorithm for altimeters that operate in the Ku band as well as in the lower frequency C band. Using σ_0 from both bands improves altimeter wave period estimations because the whole wave spectrum can be better described and therefore integral period parameters. *Quilfen et al.* [2004] use a neural network methodology to derive altimeter wave period algorithms for the dual band as well as for single Ku band signal of the Topex/Poseidon altimeter, hereafter referred to as Q04. The Q04 algorithm is an improvement over the G03 algorithm. However, the measurements must be cross calibrated to Topex/Poseidon in order to apply Q04 to data from other altimeters [*MacKay et al.*, 2008]. We did not have any data points to enable such a cross calibration. *MacKay et al.* [2008] propose a two-piece altimeter wave period model based on Ku band σ_0 and H_s performing better than both G03 and Q04, but for this model we did not have sufficient data points either as it involves five fitting parameters. *MacKay et al.* [2008] used at least 500 data pairs. Recently, *Badulin* [2014] presented a physical model for wave period from altimeter data based solely on H_s and its spatial gradient estimated from altimeter measurements in two consecutive points along the altimeter track. It does not use σ_0, so the correlation between H_s and σ_0 is not an issue. The physical model should make a satellite altimeter-specific or region-specific calibration avoidable. We chose not to use

this model, however, as it is presented as a physical concept rather than a tool for getting better quantitative agreement. In summary, wave period from altimetry is still in development and not one of the altimeter's core ocean variables; we applied the G03 algorithm because it is widely used and applicable to our small data set.

3.1.2. Deep Water Approximation

The G03 algorithm has been derived for the open ocean and is not necessarily applicable to the coast; in the following its applicability is investigated in theory. The propagation of a harmonic wave at the water surface over water depth, d, can be described by the dispersion relationship

$$\varpi^2 = gk \tanh(kd) \tag{6}$$

with angular frequency ω ($= 2\pi/T$), wave number k ($= 2\pi/L$), and $g \approx 9.8\ \mathrm{m/s^2}$ the standard gravity [*Holthuisen*, 2007]. For deep (shallow) waters equation (6) approaches equations (7) and (8),

$$L << d \quad L = gT^2/(2\pi) \tag{7}$$

$$L >> d \quad L = T\sqrt{gd} \tag{8}$$

If the depth is greater than half a wavelength, a wave is generally considered to be a deep water wave. In Farr Bay maximum wavelength for a deep water wave therefore is 120 m, leading to 8.8 s for maximum wave period (equation (7)). Higher wave periods do not occur very often [*Badulin*, 2014; *Gommenginger et al.*, 2011; *MacKay et al.*, 2008], but in that case the deep water approximation used in G03 can potentially introduce large errors. The effect of depth on G03 performance was evaluated at the comparison sites.

3.2. Wave Power

The wave power, P, in deep water is often expressed in units in power per meter of wave crest as

$$P = \frac{\rho g^2}{64\pi} H_s^2 T_E \quad (\mathrm{W/m}) \tag{9}$$

with ρ sea water density ($1025\ \mathrm{kg/m^3}$) and T_E energy period. T_E is defined by m_{-1}/m_0, the mean wave period with respect to the spectral distribution of energy. It is the equivalent to the period of a monochromatic wave whose wave height equals H_s and which has the same energy as the irregular sea in question [*Cahill and Lewis*, 2013]. T_E can be derived from T_z and for the most common Joint North Sea Wave Project form (peak shape parameter $\gamma = 3.3$)

$$T_E = 1.18 T_z \tag{10}$$

should be used [*Cahill and Lewis*, 2014]. *Cahill and Lewis* [2014] show that T_E/T_z ratios for real sea conditions are generally higher than those in theoretical relationships. Therefore, equation (9) can be used in combination with equation (10) as a first guess of the available wave power (in shortage). For more accurate estimations the observed wave spectrum should be taken into account. According to *Cahill and Lewis* [2014], T_m is increasingly used in wave energy resource assessment also. In contrast to T_E, T_m is defined as the inverse of the mean frequency with respect to the spectral distribution of energy (equation (3)).

Equation (9) is generic as there are many different devices that each can extract the wave energy from different properties of the waves. For instance, the Pelamis wave device is a line absorber or surface-following attenuator, and such design has a response to wave curvature and frequency rather than wave height [*Retzler*, 2006]. *Rusu and Guedes Soares* [2013] present a $T_E - H_s$ look-up table indicating the electric power of a Pelamis wave device in kilowatt. In this paper we will not use this Pelamis power matrix but analyze the wave power in more universal terms using equations (9) and (10) enabling a comparison between our results and those of previous studies of wave resource assessment such as the model estimations of mean wave power (calculated using T_E) presented in the UK Marine Renewable Energy Resources Atlas [*ABPmer*, 2008]. This atlas is regularly used to support decisions relating to the deployment of offshore wind, wave, and tidal technologies and other policies that concern the marine environment.

4. Results and Discussion

4.1. Wave Height

We compared altimeter wave height, $H_{s,a}$, and buoy wave height, $H_{s,b}$, for the passes 143, 687, and 876. For each pass we obtained the AltiKa measurement located closest to the buoy and paired this with the buoy

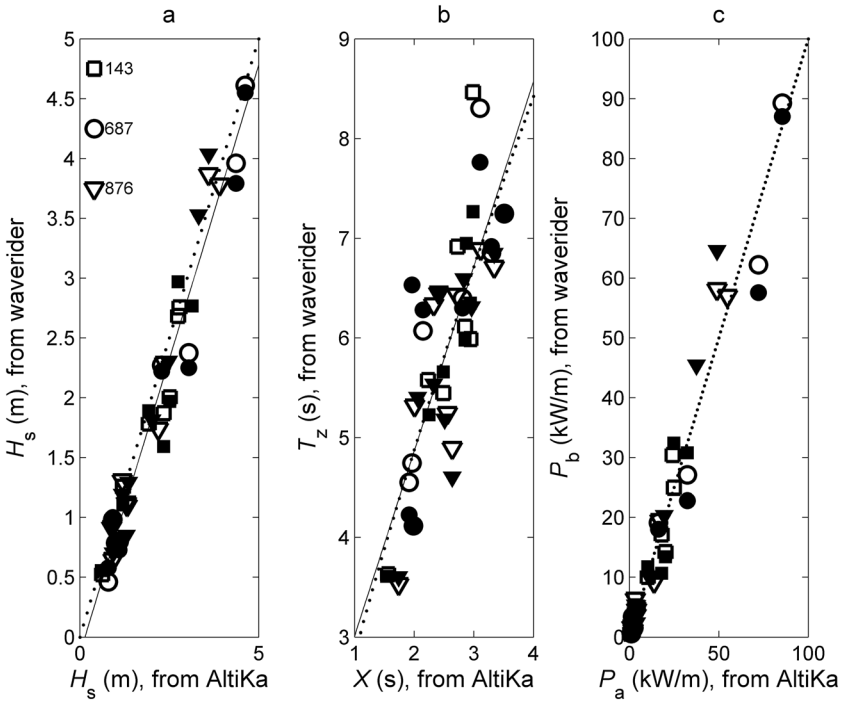

Figure 1. Scatterplots of waverider against AltiKa measurements with open (closed) symbols for eastern (western) waverider. (a) Significant wave heights; the solid line indicates a linear least squares fit (equation (11)) and the dotted line a one-on-one relation. (b) Zero-crossing period as a function of X (equation (5)); the solid line indicates a linear least squares fit (Table 1) and the dotted line a fit to a power function ($T_z = 2.82X^{0.79}$). (c) Power per meter wave crest (equation (9)); the dotted indicates a one-on-one relation.

measurement closest to the pass time. Hence, a 1 s AltiKa sample was compared with a half-hour waverider average. In total, 48 data points were obtained (24 for each buoy). The maximum distance between buoy and AltiKa sample location was 16 km, the average ± standard deviation, SD, for the eastern (western) buoy being 10 ± 2 km (8.5 ± 5 km), while the time difference was about 1 min. Buoy wave heights of the collocated data ranged between 0.46 and 4.61 m and was 1.90 m on average (the minimum, maximum, and mean wave

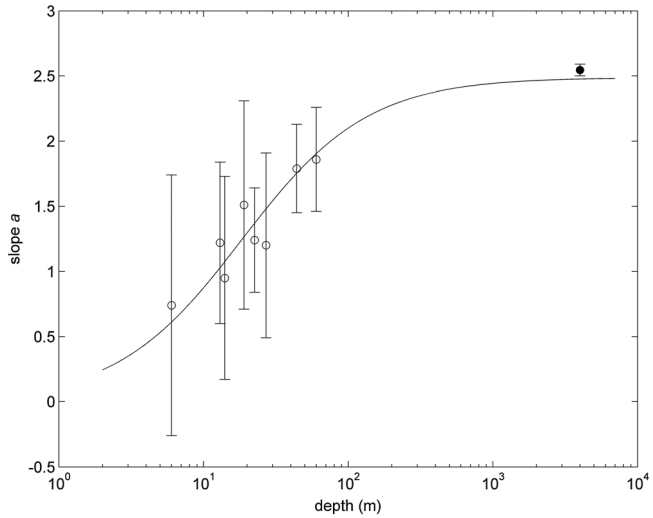

Figure 2. Scatterplot of regression slope, a, as a function of d (Table 1). Solid line shows curve fit, $a = d/(7.39 + 0.41d)$, ($R^2 = 0.9$; RMSE = 0.18) [*Silva and Silva*, 2010] with ±2.50 and ±0.06 respective uncertainties of 7.39 and 0.41 for 95% confidence bounds.

Table 2. Mean Power per Meter of Wave Crest in kW/m as Estimated by AltiKa, P_a ($P_a \pm$ se Includes Standard Error of the Mean, and P_a (95%) Includes 95% Confidence Bounds), Using AltiKa Data in the Year 2014, and the Seasonal Wave Power Ranges Presented in the UK Marine Renewable Energy Resources Atlas [*ABPmer*, 2008]

	$P_a \pm$ se	P_a (95%)	N	*ABPmer* [2008]
All	16 ± 4	16 ± 8	30	10–15
Winter	29 ± 10	29 ± 24	7	20–30
Spring	11 ± 8	11 ± 18	9	10–20
Summer	8 ± 6	8 ± 14	7	1–5
Autumn	21 ± 7	21 ± 17	7	10–20

height over all available buoy data were, respectively, 0.24, 8.44, and 1.90 m). A linear least squares fit using data from both buoys gave

$$H_{s,b} = 0.98H_{s,a} - 0.14 \tag{11}$$

($R^2 = 0.95$) with respective errors at 95% confidence levels in slope and intercept of ±0.07 and ±0.16 and an RMSE of the fit of 0.26 m (Figure 1a). The relation was not significantly different for the separate eastern and western buoys. Within the errors, the regression slope and intercept agreed well with those derived by *Sepulveda et al.* [2015]; for 3197 coastal AltiKa versus buoy measurements, outliers excluded, they found $H_{s,b} = 1.0084H_{s,a} - 0.0943$ (RMSE of 0.22 m).

For the comparison sites maximum (average) distance between in situ and AltiKa sample was 17.6 km (10 km) while the time difference was less than 30 min (8 min). The linear regressions between $H_{s,a}$ and $H_{s,b}$ were highly significant for each of the eight comparison sites with $p < 1E\text{-}04$ for the site with the lowest significance (p indicates the p value of the significance of the regression coefficient, R^2). The regression slope ranged between 0.92 and 1.08 and was 0.96 on average with no significant dependence of the relation (offset and R^2) on the water depth or distance from the shore. Mean intercept was 0.006 with ±0.13 standard deviation.

4.2. Wave Period

During the entire waverider deployment at Farr Point the measured wave periods in seconds ranged between 2.6–11.4 (T_z), 2.7–14.4 (T_m), and 3.2–22.2 (T_p). For the measurements coinciding with the AltiKa passes the respective ranges were smaller: 3.5–8.5 (T_z), 3.8–10.7 (T_m), and 3.3–15.4 (T_p), implying that equation (7) could be applied to T_z and the collocated data. However, for T_m and T_p the deep water approximation could introduce errors. Calculations of X using altimeters σ_0 and H_s were compared with coincident waverider T values according to the three definitions equations (2)–(4). The comparison showed significant relations but not as strong as the one between altimeter and waverider H_s (equation (11)). The linear least squares fit was strongest for T_z, while for T_p the correlation with X was weakest (Table 1) in agreement with *Gommenginger et al.* [2003]. The RMSE of the X-T fit for T_z, T_m, and T_p was, respectively, 0.7, 1.0, and 2.4 s. A scatterplot between X and T_z is given in Figure 1b. Fitting T_z against X in log-log space, as proposed by *Gommenginger et al.* [2003], did improve the regression coefficient of the fit slightly ($R^2 = 0.69$), but fitting T_z to a power function of X did not, so we concluded that the advancement for our data was insignificant.

We applied the linear X-T_z relationship to the data obtained for the comparison sites and found that the regression coefficients for the F3 platform (F3PFM) were not significantly different from those derived for Farr Bay (Table 1). F3PFM was the deepest of the comparison sites (44 m) and farthest from the coast but shallower than Farr Bay site. For shallower stations the regression slope, a, decreased with decreasing depth. Increasing steepness of the regression slope with increasing depth complied with the larger slope found by *Gommenginger et al.* [2003] for the open ocean data (Table 1) where the depth is ~4000 m on average. Depth dependence was to be expected as with decreasing depth the deep water approximation $L \propto T^2$ (equation (7)) transitions to $L \propto T\sqrt{d}$ (equation (8)) while the definition of X is based on the deep water approximation. The d-a curve (using our data and the measurement of *Gommenginger et al.* [2003]) is illustrated in Figure 2.

The regression offset, b, was strongly linearly related to a; using all data in Table 1, we found $b = -2.00a + 4.42$ ($R^2 = 0.97$; RMSE = 0.21), with ±0.32 and ±0.50 the respective errors at 95% confidence levels in slope and intercept. T_z could therefore be estimated by a alone:

$$Tz = aX - 2.00a + 4.42 \tag{12}$$

4.3. Wave Power in Farr Bay

The power per meter of wave crest derived from AltiKa data, P_a, was calculated using equation (9) with calibrated $H_{s,a}$ (equation (11)) and T_E from T_z (equation (10)) with $T_z = 1.86X + 1.15$ T_z (Table 1 and Figure 1c). Over all 48 data points collocating with buoy data the mean ± standard error of the mean (se = SD/√48) [*Taylor*, 1997] of P_a was 19.2 ± 3.3 kW/m. If the buoy measurements of H_s and T_z corresponding with the 48 data points were used, P_b was 19.2 ± 3.4 kW/m. (The differences between mean P_a and P_b at the location of the eastern and western buoy were insignificant.) Over all available buoy data P_b was 20.9 ± 0.07 kW/m, so the data shortage caused by the low temporal resolution of the AltiKa measurements did not introduce a significant bias in mean P over the buoys' measurement periods. If all available AltiKa measurements at the location of the eastern buoy in the year 2014 were used, the average of P_a was 16.5 ± 3.9 kW/m (not significantly different at the location of the western buoy). Table 2 shows the annual and seasonal mean values of P_a in 2014 and the corresponding ranges of P at the buoy's locations in Farr Bay presented by the UK Marine Renewable Energy Resources Atlas [*ABPmer*, 2008]. For winter and spring mean P_a fell within the ranges given in the atlas; for summer and autumn mean P_a was somewhat higher but the ranges in the atlas and in P_a overlapped. Therefore, 1 year of AltiKa data gave reasonable estimates of mean P at our location. Wave energy developers are also interested in peak power, but for capturing the wave dynamics over a 1 year period the temporal resolution of the AltiKa observations was too low. Maximum P calculated using all buoy data was 439 kW/m, while maximum P_a was 87 kW/m using all AltiKa data. *Portilla et al.* [2013] explain that the spreading of energy in frequency and direction and its seasonality also play a fundamental role in dictating what can be harvested by a given system. In conclusion, AltiKa could give a first, but not complete, estimate of the potential for a wave energy farm at a coastal location.

5. Summary and Conclusions

We could use AltiKa data to estimate wave power per meter wave crest, P, at a location 10 km off the coast. Our comparison of significant wave height (H_s) at that location, measured in situ and by AltiKa, agreed with a validation using many more coastal data points on a global scale [*Sepulveda et al.*, 2015]. Using AltiKa measurements of H_s and σ_0, we could predict zero-crossing wave period, T_z, and consequently wave energy period, T_E. Then we calculated P from H_s and T_E. The annual and seasonal mean values of P estimated using AltiKa parameters largely agreed with the P ranges presented in the UK Marine Renewable Energy Resources Atlas [*ABPmer*, 2008]. An analysis of wave data from eight comparison sites showed that at locations closer than 10 km to the coast and shallower than 60 m depth the relation between altimeter and in situ H_s did not change significantly. Here T_z could also be estimated, but the relation between AltiKa measurements and in situ measurements appeared to be depth dependent. An empirical relation was found to describe this dependence and will be subject of future study. The validity of equation (12) and the relation shown in Figure 2 needs to be assessed over intermediate depths between the coast and the ocean. The presented technique has potential to use AltiKa data for exploring wave energy resources all over the globe if the water depth is known. We can take advantage of not only the AltiKa data but also previous altimeter data that are currently being reprocessed using algorithms improved for the coastal zone.

Acknowledgments

This research is a contribution of project TURNKEY (Transforming Underutilised Renewable Natural Resource into Key Energy Yields; project 2013-1/279) of the Atlantic Area Transnational Cooperation Programme financed by the European Regional Development Fund (ERDF). The AltiKa data were generated by CNES and distributed by AVISO (ftp://avisoftp.cnes.fr/AVISO/pub/saral/gdr_t/). The wave measurement data in the Netherlands were made freely available upon request by Rijkswaterstaat, Netherlands (https://www.rijkswaterstaat.nl/formulieren/contactformulier_servicedesk_data.aspx). The wave measurement data in Farr Bay, UK, are available from the authors upon request (lonneke.goddijn-murphy@uhi.ac.uk).

The Editor thanks two anonymous reviewers for their assistance in evaluating this paper.

References

ABPmer (2008), Atlas of UK Marine Renewable Energy Resources. [Available at http://www.renewables-atlas.info/ (Date of access 11 August 2014).]

Badulin, S. I. (2014), A physical model of sea wave period from altimeter data, *J. Geophys. Res. Oceans*, *119*, 856–869, doi:10.1002/2013JC009336.

Barrick, D. E. (1974), Wind dependence of quasi-specular microwave sea scatter, *IEEE Trans. Antennas Propag.*, *AP-22*, 135–136.

Bronner, E., A. Guillot, and N. Picot (2013), SARAL/AltiKa products handbook. (No. CNES: SALP-MU-M-OP-15984-CN).

Cahill, B. G., and T. Lewis (2013), Wave energy resource characterisation of the Atlantic Marine Energy Test Site, *Int. J. Mar. Energy*, *1*, 3–15, doi:10.1016/j.ijome.2013.05.001.

Cahill, B. G., and T. Lewis (2014), Wave period ratios and the calculation of wave power, 2nd Marine Energy Technology Symposium METS2014, Seattle, Wash.

Cipollini, P., J. Benveniste, J. Bouffard, J. Emery, L. Fenoglio-Marc, C. P. Gommenginger, and J. Zavala-Garay (2010), The role of altimetry in coastal observing systems. OceanObs'09: Sustained Ocean Observations and Information for Society (Vol. 2), Venice, Italy, 21–25 Sept. 2009.

Golubkin, P. A., B. Chapron, and V. N. Kudryavtsev (2014), Wind waves in the Arctic seas: Envisat and AltiKa data analysis, *Mar. Geod.*, doi:10.1080/01490419.2014.990592, accepted.

Gommenginger, C. P., M. A. Srokosz, and P. G. Challenor (2003), Measuring ocean wave period with satellite altimeters: A simple empirical model, *Geophys. Res. Lett.*, *30*(22), 2150, doi:10.1029/2003GL017743.

Gommenginger, C., P. Thibaut, L. Fenoglio-Marc, G. Quartly, X. Deng, J. Gómez-Enri, and Y. Gao (2011), A review of retracking methods and some applications to coastal waveforms, in *Coastal Altimetry*, edited by S. Vignudelli et al., pp. 61–101, Springer, Berlin.

Holthuisen, L. H. (2007), *Waves in Oceanic and Coastal Waters*, Cambridge Univ. Press, Cambridge, U. K.

MacKay, E. B. L., C. H. Retzler, P. G. Challenor, and C. P. Gommenginger (2008), A parametric model for ocean wave period from Ku band altimeter data, *J. Geophys. Res.*, *113*, C03029, doi:10.1029/2007JC004438.

Portilla, J., J. Sosa, and L. Cavaleri (2013), Wave energy resources: Wave climate and exploitation, *Renewable Energy*, *57*, 594–605, doi:10.1016/j.renene.2013.02.032.

Queffeulou, P. (2004), Long-term validation of wave height measurements from altimeters, *Mar. Geod.*, *27*(3–4), 495–510, doi:10.1080/01490410490883478.

Quilfen, Y., B. Chapron, F. Collard, and M. Serre (2004), Calibration/validation of an altimeter wave period model and application to TOPEX/Poseidon and Jason-1 altimeters, *Mar. Geod.*, *27*(3–4), 535–549, doi:10.1080/01490410490902025.

Raney, R. K., and L. Phalippou (2011), The future of coastal altimetry, in *Coastal Altimetry*, edited by S. Vignudelli et al., pp. 535–560, Springer, Berlin.

Rascle, N., and F. A. Ardhuin (2013), A global wave parameter database for geophysical applications. Part 2: Model validation with improved source term parameterization, *Ocean Modell.*, *70*, 174–188, doi:10.1016/j.ocemod.2012.12.001.

Retzler, C. (2006), Measurements of the slow drift dynamics of a model Pelamis wave energy converter, *Renewable Energy*, *31*, 257–269, doi:10.1016/j.renene.2005.08.025.

Rusu, E., and C. Guedes Soares (2013), Coastal impact induced by a Pelamis wave farm operating in the Portuguese nearshore, *Renewable Energy*, *58*, 34–49, doi:10.1016/j.renene.2013.03.001.

Sepulveda, H. H., P. Queffeulou, and F. Ardhuin (2015), Assessment of SARAL AltiKa wave height measurements relative to buoy, Jason-2 and Cryosat-2 data, *Mar. Geod.*, doi:10.1080/01490419.2014.1000470.

Silva, W. P. D., and C. P. D. Silva (2010), LAB fit curve fitting software (nonlinear regression and treatment of data program), V 7.2.47.

Taylor, J. R. (1997), *An Introduction to Error Analysis: The Study of Uncertainties in Physical Measurements*, 2nd ed., 333 pp., Univ. Science Books, Sausolito.

Tournadre, J., J. Lambin, and N. Steunou (2009), Cloud and rain effects on AltiKa/SARAL Ka-band radar altimeter. Part I: Modelling and mean annual data availability, *IEEE Trans. Geosci. Remote Sens.*, *47*, doi:10.1109/TGRS.2008.2010130.

Zieger, S., J. Vinoth, and I. R. Young (2009), Joint calibration of multiplatform altimeter measurements of wind speed and wave height over the past 20 years, *J. Atmos. Oceanic Technol.*, *26*, 2549–2564, doi:10.1175/2009JTECHA1303.1.